Leonardo Electronic Journal of Practices and Technologies
ISSN 1583-1078
Issue 32, January-June 2018
p. 93-102

Engineering, Enviroment

Time-Dependent Ginzburg–Landau equation modelling of electron beam additive manufactured Titanium alloy

Ayorinde Tayo OLANIPEKUN [1*], Abiodun Ayodeji ABIOYE [2], Kayode Emmanuel OLUWABUNMI [3]

[1] *Department of Engineering, Prototype Engineering Development Institute Ilesa Nigeria, [National Agency for Science and Engineering Infrastructures, NASENI Abuja]*
[2] *Department of Mechanical Engineering Covenant University, Ota*
[3] *Department of Engineering, Prototype Engineering Development Institute Ilesa Nigerai, [National Agency for Science and Engineering Infrastructures, NASENI Abuja]*
E-mail(s): [1] olanipekunayo2010@yahoo.com; [2] dabioye10@gmail.com; [3] kayoxemak@yahoo.com

[*] Corresponding author, phone: +2347061541108

Received: August 01, 2017 / Accepted: May 28, 2018 / Published: June 30, 2018

Abstract

In this study, the micro-structure evolution in Electron beam additive manufacturing (EBAM) process of Ti–6Al–4V is studied using phase-field modelling. EBAM involves a rapid solidification process and the properties of a build partly depend on the solidification behaviour as well as the micro-structure of the build material. Phase-field modelling was applied to study the evolution of micro-structural scale of dendrites during the Ti-6Al-4V alloy solidification in the EBAM process. The mechanical properties of the final build parts are dependent on the solidification rate which affects the micro-structure of the material. Thus, the evolving of micro-structure plays a critical and effective role towards process parameters optimization. Recent increase in computational power allows for direct simulations of micro-structures during materials processing for specific manufacturing conditions. A MATLAB code was developed to solve the set of Time-Dependent Ginzburg–Landau equation phase field equations. The effect of under-cooling was investigated through the simulations; the greater the under-cooling, the faster the dendrite grows. The micro-structure

simulations shows the growth of primary β phase, which has a body-centred cubic crystal structure phase with four fold symmetry comparable with experimental results for the tested range.

Keywords

Additive manufacturing; Phase field modelling; Electron Beam Additive Manufacturing (EBAM); Micro-structure; Titanium alloy

Introduction

Rapid prototyping differs from additive manufacturing (AM) in that Rapid prototyping is concerned with geometrical accuracy, while additive manufacturing adds a stringent requirement for the part's mechanical properties [1]. This requirement arises from the fact that AM parts not only need to be built but also to be put into service with an expected performance [2]. In AM, several factors contribute to the ultimate mechanical properties of the part, including the manufacturing technique, the presence of porosity, incomplete melting, proper thermal control to avoid over melting, and the quality of the powder feedstock [3-6].

Additive manufacturing (AM) is the newest powder metallurgy (PM) technique [7-9] while Ti-6Al-4V is the single most important Ti alloy [10-15].

Introduction of Ti6Al4V in AM opens various opportunities to manufacture complex shapes with industrial relevance, for example, cellular structures for lightweight aircraft components, biomedical implants, offshore and marine components due to the characteristics such as high strength-to-weight ratio, good biocompatibility and excellent corrosive resistance [16-17]. The addition of 4 wt% V as the β stabiliser lowers α-to-β transition temperature; therefore, at room temperature, the microstructure of Ti-6Al-4V typically consists of a mixture of α and β phases (duplex microstructure). EBM processed Ti-6Al-4V shows greater ductility when compared to laser processed Ti-6Al-4V [18]. A majority of acicular martensites α′ have been found in the SLM Ti-6Al-4V alloy, which leads to high mechanical strength but low ductility [19]. Lutjering et al. have shown that the thickness of the "α" lath is the primary factor influencing strength and ductility [20].

Since the early 1990s, the phase-field methodology has emerged as a powerful mathematical and computational modelling technique to capture a wide variety of crystal growth and solidification structures. The phase-field methodology is based on the

construction of a Cahn–Hilliard or Ginzburg–Landau energy or entropy functional. By variational derivatives, a set of partial differential equations for the appropriate thermodynamic quantities (e.g., temperature, concentrations) with an additional reaction–diffusion equation for the phase field variable, often called the phase-field equation, can be derived from the functional [21].

There have been some initial attempts to employ the phase-field method for modelling micro-structure evolution during AM. For example, in the work of Gong et al. [22-23], they coupled the thermal process modelling with a phase-field model to simulate the dendrite morphology during AM of Ti-6Al-4V, as well considering under cooling effect. Lim et al. [24] was able to show a rather preliminary modelling framework using both the phase-field approach and a crystal plasticity finite element (CP-FE) method which could be applicable to micro-structure evolution modelling in AM. Xibing and Kevin [25] have worked on a two-dimensional finite-element analysis (FEA) thermal model of Ti-6Al-4V which was implemented in ABAQUS 6.11 to holistically study the thermal process of EBAM, the dendrite morphology at various under cooling's was simulated they observed that columnar dendritic spacing and the width of dendrites decrease with the increase of the beam scanning speed [23].

There is direct relationship between the mechanical properties and micro-structure, phase composition and physical quality, which are controlled by various processing parameters like powder flow rate, layer thickness, scan speed, laser intensity and spot size in manufacturing and subsequent heat treatments [25].

It is found that previous phase field modelling of dendritic solidification of Ti6Al4V works has not really applied the Phase field Time-Dependent Ginzburg–Landau equation.

In this study, anisotropy was implemented in the inter-facial energy and the mobility that appears in phase-field models for Ti6Al4V in the concept of the additive manufacturing process simulation, an accurate and efficient Phase field Time-Dependent Ginzburg–Landau equation for dendritic solidification of Ti6Al4V alloy was implemented. The thermophysical parameters used in the phase-field modelling are listed in Table below. The mesh size is set as 0.1 lm. The programming of dendrite growth was written in the MATLAB (The Math Works Inc., Natick, MA) to solve partial differential equations and consequently simulate the evolution of the crystal growth. The multiple dendrites growth is also simulated to validate the phase-field modelling.

Materials and method

A phase-field model describes a microstructure (both the compositional or structural domains) with a set of field variables. The field variables are assumed to be continuous across the interfacial regions, which is opposite of that in sharp interface models where they are discontinuous [26-27].

The program structure of the phase-field simulation code are presented in Figure 1.

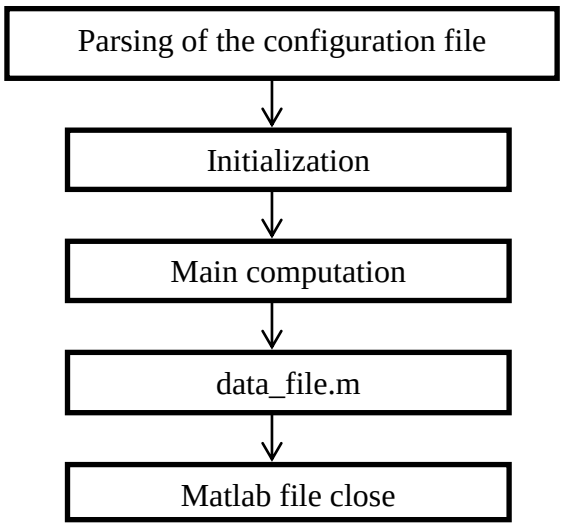

Figure 1. Program structure of the phase-field simulation code

The model given below is based on the most celebrated work of Kobayashi [28] which is one of the earliest phase-field models for the dendritic solidification. It was chosen in here for its Simplicity; the model includes two variables: one is the non-conserved phase-field parameter, φ(r, t), which takes the value of one in the solid and zero in the liquid. The other is the temperature field T(r, t) which also evolves as the solidification progresses. Of course, r is the spatial position and t is the time. In the following, Ginzburg– Landau type free energy is considered, Eq. (1):

$$F(\varphi, m) = \int_v \frac{1}{2}\varepsilon^2 |\nabla\varphi|^2 + f(\varphi, m) dv \qquad (1)$$

Where: in the integrant above, the gradient energy ε is the anisotropic gradient energy coefficient which determines the thickness of the interface layer. The second term in Equation (1) is the local free energy which is a double-well potential and has local minimums at φ = 0 and φ = 1; m - the driving force for the interface motion proportional to super cooling.

The functional form for free energy, f (φ, m), is taken as Eq. (2):

$$f(\varphi, m) = \frac{1}{4}\varphi^4 - \left(\frac{1}{2} - \frac{1}{3}m\right)\varphi^3 + \left(\frac{1}{4} - \frac{1}{2}m\right)\varphi^2 \quad (2)$$

The interfacial anisotropy is introduced by assuming that ε depends on the direction of the outer normal vector at the interface. Its value evaluated as, Eq. (3):

$$\varepsilon = \bar{\varepsilon}\sigma(\theta) \quad (3)$$

Where: ε - the mean value of ε and σ (θ) - the anisotropy.

The anisotropy is expressed as, Eq. (4):

$$\sigma(\theta)=1 + \delta\cos\left(j(\theta - \theta_0)\right) \quad (4)$$

Where: δ - is the strength of the anisotropy, j - is the mode number of anisotropy, which takes the value of four cubic lattices and six for hexagonal lattices; θ is the initial offset angle and taken as a constant.

The angle, θ, is defined as, Eq. (5):

$$\theta = tan^{-1}\left(\frac{\partial\varphi/\partial y}{\partial\varphi/\partial x}\right) \quad (5)$$

The parameter m that appears in Eq. (2), is assumed to be dependent upon the degree of super cooling and the temperature. This dependency is expressed as Eq. (6):

$$m(T) = \left(\frac{\alpha}{\pi}\right) tan^{-1}\left[\gamma(T_{eq} - T)\right] \quad (6)$$

Where: α - a positive constant and Teq - the equilibrium temperature.

The time-dependent Ginzburg–Landau or Allen–Cahn equation is assumed for the evolution, Eq. (7):

$$\tau = \frac{\partial\varphi}{\partial t} = -\frac{\delta F}{\delta\emptyset} \quad (7)$$

By taking the functional derivative of Eq. (1), the time evolution becomes, Eq. (8):

$$\tau\frac{\partial\varphi}{\partial t} = \frac{\partial}{\partial y}\left(\varepsilon\frac{\partial\varepsilon}{\partial\theta}\frac{\partial\varphi}{\partial x}\right) - \frac{\partial}{\partial x}\left(\varepsilon\frac{\partial\varepsilon}{\partial\theta}\frac{\partial\varphi}{\partial y}\right) + \nabla.(\varepsilon^2\nabla\varphi) + \varphi(1-\varphi)\left(\varphi - \frac{1}{2} + m\right) \quad (8)$$

The evolution of temperature field, T(r, t), is derived from the conservation law of enthalpy as Eq. (9):

$$\frac{\partial T}{\partial t} = \nabla^2 T + k\frac{\partial\varphi}{\partial t} \quad (9)$$

Where: T - non-dimensionalized so that the characteristic cooling temperature is zero and the equilibrium temperature is one dimension less latent heat which is proportional to the latent heat and inversely proportional to the strength of cooling.

Simulation of microstructure evolution of TI-6AL-4V in SLM process

We implement Time-Dependent Ginzburg–Landau equation for dendritic solidification of Ti6Al4V alloy. A Matlab code is developed to solve the phase field equations. A typical grid system used in this study contained 500 × 500 grid points and the corresponding computational domain has dimension of 100 μm × 100 μm in both x and y direction. The grid spacing is set to dx = dy = 0.03.

In the model, the ternary Ti-6Al-4V alloy is treated as binary and the solute is the combination of Al and V. The thermophysical parameters used in the phase-field modelling are listed in Table 1. It is assumed that the initial temperature and concentration of liquid is uniform in the calculated region. The mesh size is set as 0.15m. The programming of dendrite growth was written in the MATLAB (The Math Works Inc., Natick, MA) to solve partial differential equations and consequently simulate the evolution of the dendrite growth.

Table 1. Thermo-physical properties and parameters used in the phase-field modelling on Ti-6Al-4V [29, 30, 31, 32]

Parameters	**Value**
Initial concentration, C0 (wt. %)	10.0
Equilibrium partition coefficient, K	0.5
Liquidus slope, (K)	-0.088
Diffusion coefficient in liquid, DL ( )	$9.5E^{-9}$
Diffusion coefficient in solid, DS ( )	$5.0E^{-13}$
Interface energy, σ (J/m^2)	0.5
Anisotropy coefficient, ε	0.01-0.04
Noise factor, w	0.01-0.07
Liquidus temperature, TL (K)	1928 [33]
Solidus temperature, TS(K)	1878 [33]

Result and discussions

The program of two-dimensional dendrite growth was written and implemented in Matlab to simulate the evolution of crystal growth. The growth process of three dendrites at the temperature of 1878 K is shown in Figure 2. The snapshots correspond to the growth time of 0.01, 0.2, 0.6 and 1.7 s as shown in Figure 2(a), (b), (c) and (d). The primary, secondary, tertiary arms and the necking phenomenon was shown in Fig. 2. Dendrites grow at a faster rate along the crystal-axis directions. At the early stage, as shown in Figure 2(a) and (b), the crystallites with different orientation grew independently, The initial seed is obvious at the

centre of the domain as can be seen in Figure 2(a), In the beginning of growth, the secondary arms are not obvious. With continuous growth, the solutes accumulate at the solid/liquid (S/L) interface more intensely. Therefore in Fig. 2 (c) and 2 (d), with the increase of time, there is a coalescent and impingement of the adjacent grains. As the dendrites start to impinge, the dendrite growth is visibly inhibited. The competitive growth of these grains during solidification was observed. The simulated results showed that the solidification features are consistent and in tandem with those observed based on the dendrite growth in microstructural analysis of electron beam additive manufactured Ti–6Al–4V alloy.

As can be seen from the figures, depending on the strength of the anisotropy coefficient, either four or six primary arms develop from the initial seed. As the solution progresses, the side arms develops.

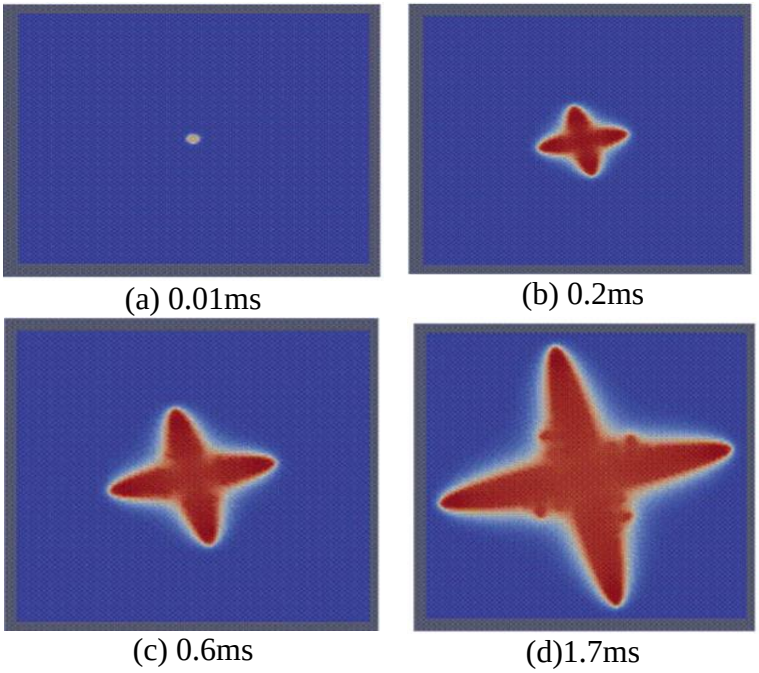

(a) 0.01ms (b) 0.2ms

(c) 0.6ms (d)1.7ms

Figure 2. Simulated dendrite structure growth at different times

It is noted that the current model is applied to model the growth of primary β phase, which has a body-centred cubic crystal structure phase with four fold symmetry.

Conclusions

The phase field method can be used to simulate the evolution of growth of primary β phase, which has a body-centred cubic crystal structure phase with four fold symmetry,

showing dendrite growth during solidification process, including primary, secondary and tertiary arms as well as the necking phenomenon.

As the time increases, the grains start to coalesce and impinge adjacent grains. As the dendrites start to impinge, the dendrite growth is visibly inhibited.

The simulation result shows arbitrarily impingement of oriented crystals and the competitive growth among the grains during solidification.

To accurately predict dendritic solidification in Ti-6Al-4V during AM, EBM additive manufacturing processing parameters, materials parameters and geometries has been imputed into the computational model. Validation through quantitative comparison with experimental results has been performed to ensure the robustness of the model. MATLAB code was used to implement and solve the phase-field equations and the phase-field model can model the morphology and solute concentration during solidification. We been able to use the model to accurately predict and reconstruct the microstructure evolution process during AM of Ti-6Al-4V. The dendritic solidification mechanisms were clearly shown in the simulation and the AM parameters that lead to the change of microstructures has been identified.

The following summarises the findings of our research:

(1) As the time increases, the grains coalesce and impinge adjacent grains. The dendritic growth is vividly seen when the dendrites start to impinge one another.

(2) Practical solidification was depicted with the simulation the impingement of arbitrarily oriented crystals in which the growth process of multiple dendrites was reproduced.

References

1. Bourell, D.L., Rosen, D.W., Leu, M.C., The roadmap for additive manufacturing and its impact, 3D Print. Addit. Manuf., 2014, 1, p. 6–9.
2. Wohlers T., ed., Wohlers Report 2015, Wohlers Assoc., Fort Collins, Colorado, 2015.
3. Rafi H.K., Karthik N.V., Gong H., Starr T.L., Stucker B.E., Microstructure and mechanical properties of Ti6Al4V parts fabricated by selective laser melting and electron beam melting, J. of Mat. Eng. and Performance, 2013, 22, p. 3872-3883.
4. Gong H., Rafi K., Starr T., Stucker B., The effects of processing parameters on defect regularity in Ti-6Al-4V parts fabricated by selective laser melting and electron beam melting; Proceedings of the 24th Annual Int. Solid Freeform Fabrication Symposium -An

Additive Manufacturing Conf.; Austin, TX, USA., 2013, 12–14, p. 424–439.

5. Zäh M.F., Lutzmann S., Modelling and simulation of electron beam melting, Prod. Eng. Res. Devel., 2010, 4, p. 15-23.
6. Tang H., Qian M., Liu N., Zhang Z., Yang G., Wang J., Effect of powder reuse times on additive manufacturing of Ti-6Al-4V by selective electron beam melting, J.O.M., 2015, 67, p. 555.
7. Kobryn P A., Semiatin S L., The laser additive manufacture of Ti-6Al-4V, JOM, 2001, 53 (9), p. 40-42.
8. Chahine G., Koike M., Okabe T., Smith P., Kovacevic R., The design and production of Ti-6Al-4V ELI customized dental implants, JOM, 2008, 60 (11), p. 50-55.
9. Ivanova O., Williams C., Campbell T., Additive manufacturing (AM) and nanotechnology: promises and challenges, Rapid Prototyping Journal, 2013, 19 (5), p. 353-364.
10. Froes F.H., Eylon D., Powder metallurgy of titanium alloys, Int. Materials Rev., 1990, 35 (1), p. 162-184.
11. Imam M.A., Froes F.H.S., Low cost titanium and developing applications, JOM, 2010, 62 (5), p. 17-20.
12. Qian M., Cold compaction and sintering of titanium and its alloys for near net shape or preform fabrication, Int. Journal of powder metallurgy, 2010, 46 (5), p. 29-44.
13. Ivasishin O.M., Anokhin V.M., Demidik A.N., Savvakin, D.G., Cost effective blended elemental powder metallurgy of titanium alloys for transportation application, Key Engineering Materials, 2000, 188, p. 55-62.
14. Ding R., Guo Z.X., Wilson A., Microstructural evolution of a Ti–6Al–4V alloy during thermomechanical processing, Materials Science and Eng., 2002, A327, p. 233–245.
15. Hongtao W., Zak Fang Z., Sun P., A critical review of mechanical properties of powder metallurgy titanium. International Journal of powder metallurgy, 2010, 46 (5), p. 45-57.
16. Campanelli S.L., Contuzzi N., Ludovico A.D., Caiazzo F., Cardaropoli F., Sergi V., Manufacturing and characterization of Ti6Al4V lattice component manufactured by selective laser melting, Materials, 2014, 7, p. 4803.
17. Donachie M J., Titanium: a technical guide, Materials Park, OH: ASM Int., 2000.
18. Hermann R.K., Sven O., Nowotny S., Laser cladding of the titanium alloy TI6242 to restore damaged blades, Proc.of Int.Cong.onApp. of Lasers and El.-Opt., 2004, p. 1–10.
19. Lore T., Verhaeghe F., Craeghs T., Humbeeck J.V., Kruth J.P., A study of the

microstructural evolution during selective laser melting of Ti–6al–4V, Acta materialia, 2010, 58 (9), p. 3303-3312.

20. Lütjering G., Influence of processing on microstructure and mechanical properties of (α+β) titanium alloys, Materials Science and Engineering A, 1998, 243, p. 32-45.
21. Langer J.S., Directions in Condensed Matter Physics, World Sci., Singapore, 1986.
22. Gong H., Rafi K., Gu H., Janaki Ram G D., Starr T., Stucker B., Influence of defects on mechanical properties of Ti–6Al–4V components produced by selective laser melting and electron beam melting, Materials & Design, 2015, 86, p. 545-554.
23. Gong X B., Chou K., Phase-field modelling of microstructure evolution in electron beam additive manufacturing, JOM, 2015, 67, p. 1176-1182.
24. Lim H., Abdeljawad F., Owen S.J., Hanks B.W., Foulk J.W., Battaile C.C., Incorporating physically-based microstructures in materials modelling: Bridging phase field and crystal plasticity frameworks, Modell. Sim. Mat. Sci. Eng., 2016, 24.
25. Krol M., Tanski T., Surface quality research for selective laser melting of Ti-6Al-4 Valloy, Arch Metall Mater, 2016, 61 (3), p. 1291–1296.
26. Cahn J.W., Hilliard J.E., Free energy of a non-uniform system, I. Int. en. J. Chem Phys, 1958, 28, p. 258.
27. Cahn J.W., On spinodal decomposition. Acta Metall, 1961, 9, p. 795.
28. Kobayashi R., Modelling and numerical simulations of dendritic crystal-growth. Physica, 1993, D63, p. 410.
29. Miller M.K., Russell K.F., Embrittlement of RPV steel: an atom probe tomography perspective, J. Nucl. Mater., 2007, 371, p. 145.
30. Nastac L., Solute redistribution liquid/solid interface and initial transient regions during the unidirectional solidification of Ti-6-4 and Ti-17 alloys, CFD modelling and simulation in materials processing, TMS, 141st Ann. Meet., Orlando, 2012, p. 11-15.
31. Rai R., Elmer J.W., Palmer T.A., DebRoy T., Heat transfer and fluid flow during keyhole mode laser welding of tantalum, Ti-6Al-4V, 304L stainless steel and vanadium, J. Phys. D Appl. Phys., 2007, 40 (18), p. 5753-5766.
32. Suzuki T., Ode M., Kim S.G., and Kim W.T., Phase-field model of dendritic growth, J. Cryst. Growth, 2002, 237–239, p. 125–131.
33. Kim S.G., Kim W.T., Suzuki T., Phase-field model for binary alloys, Phys. Rev., 1999, E 60, p. 7186.